

Tunnel and thermal c -axis transport in BSCCO in the normal and pseudogap state.

M Giura^{†||}, R Fastampa[†], S Sarti[†], N Pompeo[‡], E Silva[‡]

[†] Dipartimento di Fisica and Unità CNISM, Università “La Sapienza”, Piazzale Aldo Moro 2, I-00185 Roma, Italy

[‡] Dipartimento di Fisica “E. Amaldi” and Unità CNISM, Università Roma Tre, Via della Vasca Navale 84, I-00146 Roma, Italy

Abstract. We consider the problem of c -axis transport in double-layered cuprates, in particular with reference to $\text{Bi}_2\text{Sr}_2\text{CaCu}_2\text{O}_{8+\delta}$ compounds. We exploit the effect of the two barriers on the thermal and tunnel transport. The resulting model is able to describe accurately the normal state c -axis resistivity in $\text{Bi}_2\text{Sr}_2\text{CaCu}_2\text{O}_{8+\delta}$, from the underdoped side up to the strongly overdoped. We extend the model, without introducing additional parameters, in order to allow for the decrease of the barrier when an external voltage bias is applied. The extended model is found to describe properly the c -axis resistivity for small voltage bias above the pseudogap temperature T^* , the c -axis resistivity for large voltage bias even below T_c , and the differential dI/dV curves taken in mesa structures.

PACS numbers:

^{||} E-mail:maurizio.giura@roma1.infn.it.

1. Introduction

The c -axis conductivity in layered superconductors is at the same time a fascinating puzzle and a source of interesting information on the nature of high- T_c cuprates. Focussing on $\text{Bi}_2\text{Sr}_2\text{CaCu}_2\text{O}_{8+\delta}$ (Bi:2212), on passing from underdoping to overdoping, the c -axis resistivity ρ_c changes from monotonically decreasing from T_c to high temperature to a non-monotonic behaviour, displaying a minimum at a temperature usually higher than the pseudogap temperature T^* [1, 2, 3]. This latter feature has led to a description in terms of tunnelling phenomena along the c -axis accompanied by some kind of charge localization on the ab planes [4, 5]. Such localization becomes even stronger in the so-called pseudogap phase [6], as testified by an increase of ρ_c and a change of slope in the in-plane resistivity (ρ_{ab}) [1].

In addition to the study of the c -axis resistivity, many investigations have been devoted to the study of the nonlinear electrical response exhibited by the $I - V$ characteristic [7, 8], dI/dV curves [9, 10, 11, 12], ρ_c at high applied voltages [13] or a combination of such measurements [14]. While in general terms it is fair to say that by means of such measurements one can get information both on the normal state underlying the pseudogap state and on the pseudogap state itself as well as on the superconducting state quasiparticle response, the discussion on such data is still very active [15].

Confining for the moment our attention to some feature of the measurements taken in artificially patterned mesa structures, the so called “Intrinsic Tunnelling Spectroscopy”, we recall some of the results that are particularly pertinent to the present work. In overdoped and optimally doped BSCCO mesas [13, 14], composed by several unit cells, the differential conductivity exhibits two distinct behaviours for voltages higher than a characteristic value, $V > V_g$, and for small (vanishing) voltages, $V \rightarrow 0$. The ($V \rightarrow 0$) behaviour usually regarded as originating from quasiparticles, but the strangest features came from the large voltage behaviour indicated as “normal” resistance R_N . In fact, it was found that R_N was linear in T down to $T \rightarrow 0$, in contrast with the usual behaviour of ρ_c . This feature does not seem to have been satisfactorily described.

In two recent papers [3, 16] we have addressed the issue of the out-of-plane, normal state ρ_c resistivities within a phenomenological model for bilayer superconductors, based on the existence of two energy barriers with different height and width, over which the electrical transport was determined by two complementary processes, namely incoherent tunnelling [5] and thermal activation across the two barriers. In spite of the simplicity of the model, we have been able to fit a very wide set of ρ_c data taken in BSCCO following the change of the temperature dependence of the c -axis resistivity with increasing doping δ . More precisely we showed that:

- (i) For $T > T^*$ the model (which explicitly refers to the genuine normal state, with an electron density of states that is uniform in energy) was able to describe the ρ_c data with a reduced number of fitting parameters, with a direct physical interpretation. The accuracy of the fit was as good in the underdoped region as in the overdoped one.
- (ii) For $T_c < T < T^*$, using the normal c -axis resistivity as determined by our model, we

described the loss of conductivity in the pseudogap state by a reduction of the effective number of charge carriers. We obtained the fraction $\eta(T)$ of the “gapped” carriers that do not participate to the conduction along the c -axis, defined through

$$\sigma_c = \sigma_{c,n}[1 - \eta(T)] \rightarrow \rho_c(T) = \frac{\rho_{c,n}(T)}{1 - \eta(T)} \quad (1)$$

and we found that the curves $\eta(T)$ at different dopings could be scaled onto a universal curve [16, 17].

In this paper we extend the analysis of the data by means of the proposed model, by extending it to nonzero voltages, thus allowing a comparison of the model with the data taken on the mesa structures. The main result of this paper will be a comprehensive and satisfactory explanation of the mesa resistivity branches, both for $V \rightarrow 0$ (R_0) and for $V > V_g$ (R_N).

The paper is organized as follows. In the next Section, we introduce the basic idea of the two-barrier model. We extend the model to finite applied voltage, and we discuss the limiting forms. In Sec.3 we compare the model to a variety of measurements taken at various T on BSCCO crystals. Conclusions are reported in Sec.4

2. Two-barrier model

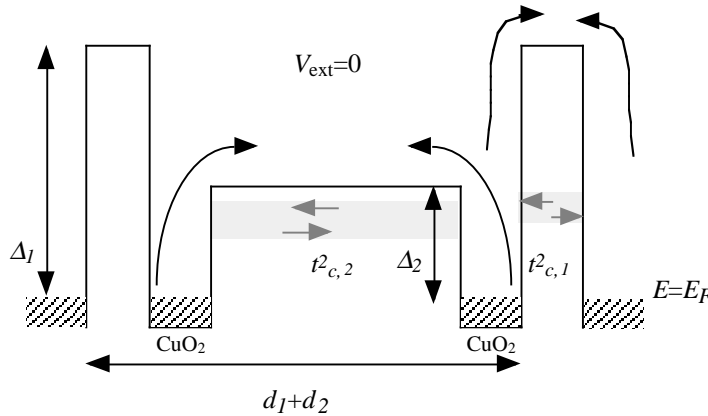


Figure 1. Sketch of the energy profile used to develop the model for the small voltage c -axis resistivity. The different processes (thermal activation and tunnelling) and heights Δ_i and widths d_i of the barriers are depicted. The barriers can be thought of as arising from the Ca layer and the Sr-Bi-Bi-Sr block, respectively.

As already mentioned, in two recent papers [3, 16] we have presented a phenomenological model for the out-of-plane resistivity ρ_c in bilayer superconductors. In this model the temperature dependence of the c -axis resistivity in the genuine normal state ($T > T^*$, where T^* indicates the pseudogap opening) arises from the existence of two different energy barriers along the c -axis, taken of rectangular shape with different heights (Δ_1 and Δ_2 , as measured from the Fermi level) and widths d_1 and d_2 , as depicted

in Fig.1. In this spatial energy landscape, in the normal state two mechanisms (for each barrier) contribute to the interlayer transport: (i) thermal activation of the carriers above the barrier (ii) tunnelling of the charge carriers partially inhibited by incoherent in-plane scattering.

The tunnelling contribution over each of the barriers was identified as given by the model of Ref.[5], for which the tunnelling contribution to the *c*-axis resistivity is modified by the existence of the interplanar incoherent scattering, leading to a confinement of the charge carriers in the *a, b* planes. In this model, the in-plane phononic, inelastic scattering, with characteristic time τ , reduces the tunnelling matrix element t_c to $(2\tau/\hbar)t_c^2 \ll t_c$ when τ is much smaller than the time between two tunnelling elements. These features of the model imply a relation between the in-plane and the out-of-plane resistivities. The overall expression for the normal state effective resistivity along the *c*-axis, $\rho_{c,n}$, is obtained as a function of the in-plane $\rho_{ab,n}$ from the series of the two barriers [3]:

$$\begin{aligned}\rho_{c,n} &= \frac{1}{d_1 + d_2} \sum_{i=1,2} \left[\frac{t_{c0,i}^2}{a\rho_{ab,n} + b} + \beta e^{-\Delta_i/k_B T} \right]^{-1} \\ &= \sum_{i=1,2} \frac{d_i}{d_1 + d_2} \left[\frac{1}{\rho_{tun,i}} + \frac{1}{\rho_{th,i}} \right]^{-1}\end{aligned}\quad (2)$$

where the last equality defines the tunnelling ($\rho_{tun,i}$) and thermal ($\rho_{th,i}$) resistivities of the *i*-th barrier, respectively, the term $a\rho_{ab,n} + b$ takes into account the increased localization due to the in-plane phononic scattering and d_i ($i = 1, 2$) is the spacing between the layers (we have taken $d_1 = 3 \text{ \AA}$, $d_2 = 12 \text{ \AA}$, the bilayer and the Sr-Bi-Bi-Sr block thickness, respectively). In this expression $t_{c0,i}^2 \propto \exp[-2d_i\sqrt{2m^*\Delta_i}/\hbar]$ (with $m^* = 4.6m_e$ [18]) and Δ_i is the height of the *i*-th barrier. Since the in-plane resistivity $\rho_{ab,n}$ is independently measured, Eq.2 contains five adjustable parameters: $a, b, \beta, \Delta_1, \Delta_2$, with the additional constraint that $\Delta_1 - \Delta_2$ is doping-independent. $t_{c0,i}^2$ is determined by d_i, Δ_i, m^* , with its prefactor absorbed in a and b . Note that a, b, β can be combined in such a way that only two of them determine the shape of the fitting curve, while the third affects the fit only through a scale factor.

In order to avoid unnecessary complications, we recall that the thermal contribution to the higher barrier (1) was found to be negligible [3], with $\Delta_1/k_B > 2000K$, so that for this barrier we can safely assume $\rho_1 \sim \rho_{tun,1}$ in the whole temperature range explored ($T < 300K$). The reference expression for the effective resistivity then simplifies to:

$$\rho_{c,n} = \frac{1}{d_1 + d_2} \left(\rho_{1,tun}d_1 + \frac{\rho_{2,tun}\rho_{2,th}}{\rho_{2,tun} + \rho_{2,th}}d_2 \right) \quad (3)$$

In Figure 2 we present a sketch of the resulting temperature dependence of the *c*-axis normal state resistivity $\rho_{c,n}$. A thorough discussion of the parameters involved in equation 2, and of their dependence on doping δ has been given in a previous paper [3]. However, it is interesting to plot separately the various contributions to the overall resistivity, $\rho_{tun,i}$ and $\rho_{th,i}$.

In particular, equation 3 predicts for $\rho_{c,n}$ the following general behaviour: at very low

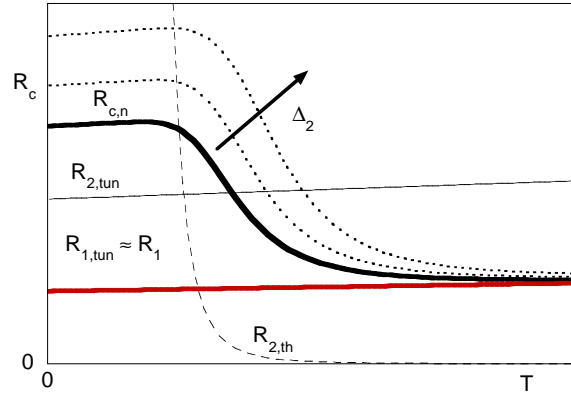


Figure 2. General overview of the temperature dependence of the c -axis resistance as calculated in the two-barrier model (black thick line), $R_{c,n} = \rho_{c,n} \frac{d_1+d_2}{S}$, where S is the transverse section. Here we have neglected (see text) the thermal conductivity across the higher barrier. The contributions of the first barrier (red thick line) and the thermal (dashed line) and tunnel (thin continuous line) contributions of the second barrier are separately plotted ($R_{i,tun} = \rho_{i,tun} \frac{d_i}{S}$ for the tunnelling resistance of each barrier, and similarly for the thermal contribution). We also report the effect of increasing Δ_2 (dotted lines).

T , $\rho_{2,th} \gg \rho_{2,tun}$, so that $\rho_{c,n}$ is substantially the sum of the two tunnelling resistivities $\rho_{1,tun}$ and $\rho_{2,tun}$, both of them linearly increasing as a function of T . As a result, $\rho_{c,n}$ increases linearly with T at low temperatures. At intermediate T , $\rho_{2,th} < \rho_{2,tun}$ so that in this temperature region the resistivity of the barrier 2 is dominated by the thermal activation term and is thus decreasing with T , and so is also the overall $\rho_{c,n}$. Finally, at high T $\rho_{2,th} \rightarrow 0$, so that $\rho_{c,n} \simeq \rho_{1,tun}$, again increasing linearly with T . The crossover from thermally activated ($\rho_{c,n} \sim \rho_{2,th}$) to tunnel dominated behaviour ($\rho_{c,n} \sim \rho_{1,tun}$) occurs for $\Delta_2/k_B T \sim 1$. It is interesting to note that this crossover reproduces in a natural way the minimum experimentally found in measurements of ρ_c in optimal and overdoped samples, assigning it to a smaller Δ_2 with respect to underdoped samples. In this framework, the minimum is not a manifestation of the opening of the pseudogap, which occurs at a lower temperature. We stress that, as mentioned in [3], the fits of ρ_c (at low voltages) only allow us to set a lower bound for $\Delta_1 - \Delta_2$.

A second interesting feature of the model is that it naturally leads to c -axis resistance linear in T at low temperature, as observed in mesa structures at high voltage bias (that is for applied voltages $V > V_g$, where V_g is a typical voltage applied to the mesa structure above which the $I - V$ curve becomes approximately linear). These data are reported, e.g., in Fig.2 of Ref.[13] and in Fig.1 (inset) of Ref.[14].

Within our model, as the voltage is increased the effective height of the second barrier decreases (see also below) while the much higher first barrier remains substantially unaffected. As a result, both the thermal and tunnelling resistivities of the second barrier become much smaller than their zero voltage values, so that the high voltage

resistivity approaches the tunnelling value $\rho_{1,tun}$:

$$R_N = R(V > V_g) \simeq R_{1,tun} = \frac{a\rho_{ab} + b}{t_{cl}^2} \frac{1}{S} \quad (4)$$

(S is the cross-section of the mesa structure) which, due to the linear dependence (as a function of T) of the in-plane resistivity directly explains the (so far unexplained) linear behaviour of R_N , as observed in mesa structure data [13, 14].

In the following, we analytically extend our model to nonvanishing voltages V , in order to compare the predictions with the large amount of data taken on mesa structures.

To be quantitatively applied to measurements of the nonlinear resistance, $I - V$ and dI/dV characteristics, the model requires a generalization that includes a direct effect of the applied voltage on the barrier height. In this case the rectangular barrier framework is no longer appropriate and a more accurate modelling of the barrier must be performed in order to take into account the decreasing of the barrier height with the external electric field. As depicted in Fig.3, we have chosen parabolic barriers since this choice allows for analytical results ¶. The energy profile along the c -axis (x direction) is then given by two parabolic barriers with the shape: $U_i(x) = U_{ci} - \frac{\alpha}{2}(x - \frac{d_i}{2})^2$ in the interval $0 < x < d_i$, and zero otherwise. The parameter $U_{c,i}$ is directly related to the previously defined height of the barrier Δ_i through the relation $U_{c,i} = \Delta_i + E_F$ (see also figure 3), while $\alpha = 8U_{ci}/d_i^2$. We stress that the choice of parabolic barriers, given the same widths d_i as in the rectangular barriers, does not introduce additional parameters.

Now we describe the different transport processes in the finite voltage regime. We

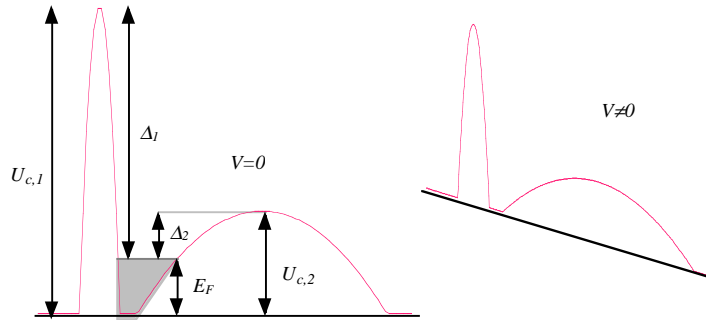


Figure 3. Left panel: generalized two-barrier model for the study of linear and nonlinear resistivity. The parabolic shape of the barrier is one of the possible choices that have to be selected, in order to incorporate in the model the reduction of the barrier height due to an external bias (finite voltage). The effect of the external voltage is sketched in the right panel.

consider first the activation process. In the presence of an external electric field \mathcal{E} , the

¶ Many other choices are clearly possible. We mention that we have performed the calculations and fittings also with trapezoidal barriers, obtaining the same results as for the parabolic case, with slightly varied numerical factors in the parameters.

barrier becomes $U'_i(x) = U_i(x) - e\mathcal{E}x$. Assuming that the volume density of carrier $n = \text{const}$ outside the barrier, the thermal charge current density is [19]:

$$J_{th,i} = -\frac{eDn(1 - e^{eV_i/k_BT})}{\int_{x_{i,1}}^{x_{i,2}} e^{[U'_i(x)-E_F]/k_BT} dx} \quad (5)$$

where D is the diffusion coefficient and V_i is the voltage drop across the i -th barrier. Thus, one has:

$$\int_{x_{i,1}}^{x_{i,2}} e^{[U'_i(x)-E_F]/k_BT} dx = e^{\Delta_i/k_BT} \int_{x_{i,1}}^{x_{i,2}} e^{-\left[\frac{\alpha}{2}(x-\frac{d_i}{2})^2 + e\mathcal{E}x\right]/k_BT} dx \quad (6)$$

where \mathcal{E} is the electric field. The integral on RHS can be expressed in terms of the error function $\Phi(x) = \frac{2}{\pi} \int_0^x e^{-t^2} dt$, and after some straightforward calculation one gets the contribution of the activation to the diffusion transport current for a single barrier:

$$J_{th,i} = -\sqrt{\frac{16U_{ci}}{\pi k_BT}} \frac{eDn(1 - e^{eV_i/k_BT}) \sinh(eV_i/2k_BT)}{d_i \exp\left[\frac{(eV_i)^2}{16U_{ci}k_BT}\right] 2\Phi\left(\sqrt{\frac{(4U_{ci}-eV_i)^2-16E_FU_{ci}}{16U_{ci}k_BT}}\right)} \quad (7)$$

In considering the tunnel resistivity, we make use of the expression

$$J_i(V_i) = -\int_0^{\Delta_i+E_F} \frac{t_{ci}^2(E)}{e(a\rho_{ab} + b)} [f(E) - f(E + eV_i)] dE \quad (8)$$

as for the field emission effect with the additional localization considered in reference [5], which we assume to be valid also in the nonlinear regime. Here $t_{ci}^2(E)$ is the (energy dependent) transparency of the barrier and f is the Fermi function. To calculate $t_{ci}^2(E)$, we use the same barrier's profile $U(x)$ used to calculate the thermal contribution. For a generic energy level E in an external field the barrier's profile is shown in Fig.3. After some calculation [20, 21], one has:

$$\begin{aligned} t_{ci}^2(E) &= \exp \left\{ -\frac{2\sqrt{2m^*}}{\hbar} \int_{x_{i,1}}^{x_{i,2}} \left[\frac{\alpha}{2}x^2 + \left(\frac{\alpha d_i}{2} - e\mathcal{E}_i \right) x - E \right]^{1/2} dx \right\} \\ &= \exp \left\{ -\frac{\pi\sqrt{2m^*U_{c,i}d_i}}{4\hbar} \left[\left(1 - \frac{eV_i}{4U_{c,i}} \right)^2 - \frac{E}{U_{c,i}} \right] \right\} \end{aligned} \quad (9)$$

for $E < U_{ci} \left(1 - \frac{eV_i}{4U_{ci}} \right)^2$ and $t_{ci}^2 = 1$ otherwise. Here \mathcal{E}_i is the electric field on the i -th barrier. The total current in the series of the two barriers is the sum of the various contributions each with its specific values of the parameters.

It must be noted that, in the nonlinear regime, several complications arise. First of all, the energy dependences of the current densities (thermal and tunnelling) is very complex by itself, and additionally due to the very similarity of the energy scales involved: the energy E , the Fermi level E_F and, in some ranges, the thermal energy k_BT are all of the same order of magnitude. A second, more subtle complication is due to the nature of the double barrier: the experimentally controlled parameter is the external potential V , applied at the series of two barriers (assuming, as in measurements of the mesa structures, that one knows the number of junctions N involved, the applied voltage

is just NV). However, V is *not* the voltage across each barrier, but the sum of the potential drops over the two barriers: $V = V_1 + V_2$. Due to the temperature and to nonlinear effects, the ratio V_1/V_2 is not constant. One can implicitly obtain each V_i by requiring that the total current through the two barriers be the same: $J = J_1 = J_2$, with $J_i = J_{th,i} + J_{tun,i}$ (the cross section S is the same throughout the sample). One can thus solve numerically to obtain V_1 and V_2 as a function of V and the $I(T, V) = JS$ and $R_c(T, V) = V/I$ for every temperature and arbitrary V .

We are now in the position to perform some comparison between the model here developed and the data for the c -axis transport. The next Section is dedicated to this task.

3. Comparison with experiments

In this Section we report the application of the model developed in Sec.2, based on parabolic barriers, to experimental data for c -axis transport in BSCCO reported in the literature or measured in our laboratory. We first analyze the data for the c -axis resistance taken in optimally doped BSCCO single crystal mesa structures [14]. Since those data were taken at small ($V \rightarrow 0$) and large ($V = V_g$) voltages, the simultaneous fitting of both sets of data allows a precise determination of the doping-independent value of $\Delta_1 - \Delta_2$. Once determined, this value will be kept fixed in the fits of all the other data at various dopings.

Due to the illustrative nature of these fittings, we describe in some detail the procedure

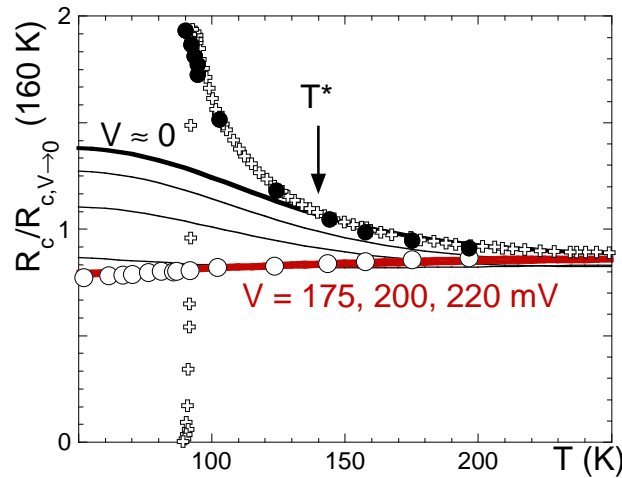


Figure 4. Normalized data for the c axis resistivity as reported in [14] at high voltage, R_{c,V_g} , open circles, and small voltage, $R_{c,V \rightarrow 0}$, full dots, compared to our data for in a BSCCO single crystal with nominal $\delta = 0.255$ (crosses). Continuous curves show the voltage bias dependence of R_c , calculated on the basis of the model described in Sec.2 with $\Delta_2/k_B = 690$ K: thick black line, $V \simeq 0$; thick red lines: $V = 175, 200, 220$ mV; thin lines, from top to bottom: 45, 90, 160 mV.

that we followed in order to reduce the number of fitting parameters. For the small

voltage resistivity, we have to refer to Eq.2, which contains the in-plane resistivity ρ_{ab} . Since those data were not available in [14], we compared the out-of-plane resistance with our data taken in BSCCO single crystals at various doping δ by an eight terminal contact method, which allows us to extract simultaneously ρ_c and ρ_{ab} [2]. As reported in Fig.4, our data for a crystal with nominal doping $\delta = 0.255$ coincides with the $R_{c,V \rightarrow 0}$ data in [14] within an overall scale factor. We then decided to use our data for ρ_{ab} in the fitting. By adjusting Δ_2 , β , a and b it is possible to fit well the normal state $R_{c,V \rightarrow 0}$ down to a temperature T^* where the pseudogap opens (we come back to this point below, see also [3, 16, 17]). For the data of R_{c,V_g} one has to refer to the complex procedure described in Sec.2, calculating the total J with the dynamic voltage partition between the two barriers. In this case the fit is sensitive to Δ_1 . In Eqs 5,6,7,8 we have used $E_F/k_B = 1000$ K [18]. By simultaneously fitting $R_{c,V \rightarrow 0}$ and R_{c,V_g} a strong constraint is put on the parameters. We found that it was indeed possible to fit *both* $R_{c,V \rightarrow 0}$ and R_{c,V_g} (a nontrivial result) with the choice $(\Delta_1 - \Delta_2)/k_B = 2000$ K, of the same order of magnitude but smaller than the value ~ 5000 K estimated in our previous works. We remark that no additional or hidden parameters are required, besides those above mentioned. In Fig. 4 we report the evolution of the nonlinear R_c at various voltages. It is seen that the fitting of R_{c,V_g} is obtained with $V = 180$ mV, as compared to $V_g \simeq 150$ mV reported in [14].

As a second illustration of the applicability of the model, we present in Fig. 5 the fits of the small voltage resistivity, $\rho_{c,V \rightarrow 0}$, as measured by us in BSCCO single crystals. In these fits we have taken $(\Delta_1 - \Delta_2)/k_B = 2000$ K, as indicated by the simultaneous fittings above performed. Thus, once a simultaneous fit of low and high voltage resistance has been performed at a single doping, the fits at all the other dopings contain only four adjustable parameters (one of which acts as a scale factor only, see Sec.2). As can be seen, the fits capture the minimum of ρ_c . The behaviour of the parameters as a function of the doping has been already discussed [3]. Here, we recall that the fits depart from the data when the pseudogap opens. In this case from Eq. 1 one can evaluate the fraction η of the carriers that no more participate to the conduction below T^* . It is not the purpose of this paper to discuss the behaviour of η , that has been partially discussed before [16] and elsewhere [17]. However, for completeness we report some of the resulting η in the inset of Fig. 5.

As a third and final illustration we calculate the differential dI/dV curves by means of the nonlinear equations 5,6,7,8 and we compare the result with the data measured in BSCCO mesa structures in [11]. The discussion of dI/dV data is of particular interest, since the “dip and hump” structure has been the subject of many discussions [9, 11, 22, 23, 24]. In particular, the survival of this structure at high temperatures is not yet unanimously attributed to some specific mechanism, and it is often interpreted as a persistence of the pseudogap at high temperatures [25].

Calculations of the dI/dV vs. V curves using our model are reported in Fig. 6. In order to compare the calculations with the data in [11], the curves have been shifted vertically. It is clearly seen that, within a single scale factor of order 1, our calculation

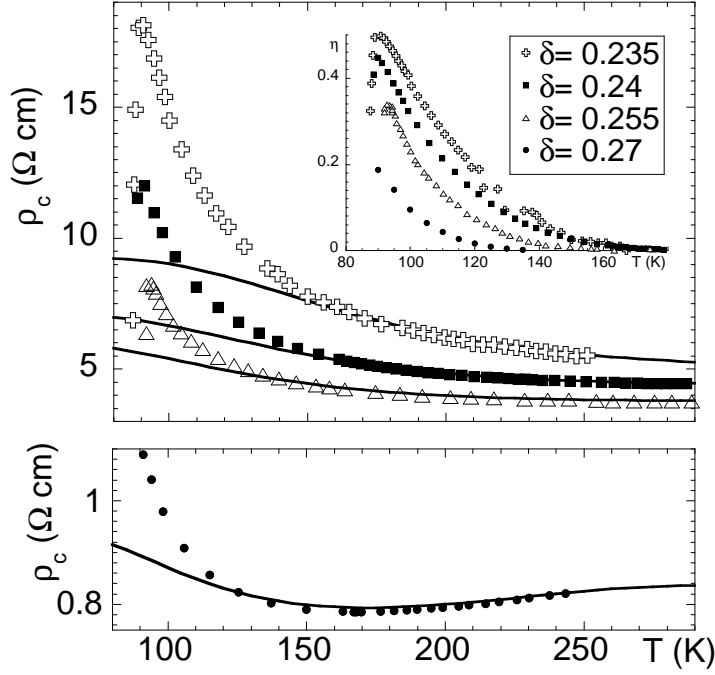


Figure 5. Typical fits of the c axis resistivity at small voltage with the proposed model, continuous lines, compared to our data in BSCCO single crystals at various dopings (symbols). The data for the most overdoped sample are reported in the lower panel with a much enlarged scale to show the minimum in ρ_c . In the inset we report the fraction of charge carriers that do not participate to the conduction after the pseudogap opening.

captures reasonably well the experimental behaviour, at all temperatures. We stress that, once a single parameter set has been chosen for one of the curves, the others are calculated without further adjustments. The agreement is fairly good, especially taking into account the very simple (albeit analytically cumbersome) model.

4. Conclusions

In this paper we have reviewed the two-barrier model for the electric transport along the c -axis in the double-layered superconductor BSCCO. We have extended the model to nonvanishing voltage bias, in order to compare the calculation with the measurements of the c -axis resistance taken in mesa structures. These measurements show rich and peculiar behaviour, namely the minimum in $\rho_c(T)$ at some doping, the crossover from concave upward $R_{c,V \rightarrow 0}(T)$ to linear R_{c,V_g} at high voltage bias, the shape of the dI/dV vs. V curves above T_c . Nevertheless, quantitative fits to all these behaviours may be obtained using a simple extension of our earlier model. It seems that double-layered tunnelling might be responsible or co-responsible for many of the experimental observations.

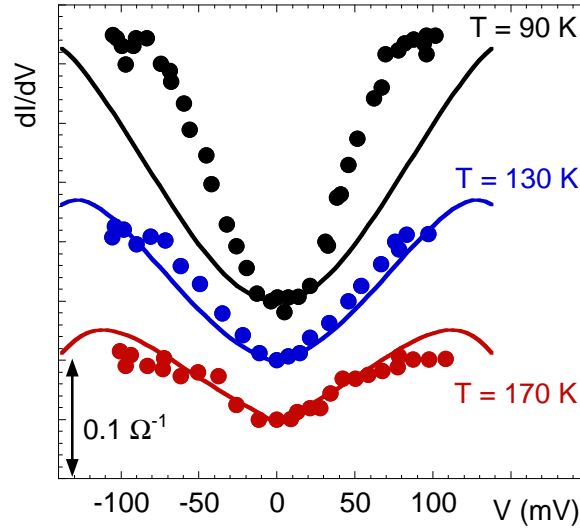


Figure 6. Differential conductance dI/dV vs. V in a sample with $\delta = 0.25$; symbols: experimental data after [11]; continuous lines: fits by means of the model described in Sec.2. The calculated curves have been scaled by a single overall factor. The curves have been shifted vertically for clarity.

Acknowledgments

We are grateful to E. L. Wolf and G. Gu for supplying the BSCCO crystals whose data are reported in Fig.5.

References

- [1] Watanabe T, Fujii T and Matsuda A 1997 *Phys. Rev. Lett.* **79** 2113
- [2] Esposito M, Muzzi L, Sarti S, Fastampa R and Silva E 2000 *J. Appl. Phys.* **88** 2724
- [3] Giura M, Fastampa R, Sarti S and Silva E 2003 *Phys. Rev. B* **68** 134505
- [4] Anderson P W 1997 *The theory of Superconductivity in the High- T_c cuprates* (Princeton Series in Physics)
- [5] Kumar N and Jayannavar A M 1992 *Phys. Rev. B* **45** 5001
- [6] Timusk T and Statt B 1999 *Rep. Prog. Phys.* **62** 61
- [7] Tanabe K, Hidaka Y, Karimoto S, Suzuki M 1996 *Phys. Rev. B* **53** 9348
- [8] Schlenga K, Kleiner R, Hechtischer G, Möfle M, Schmitt S, Müller P, Helm Ch, Preis Ch, Forsthofer F, Keller J, Johnson H L, Veith M, Steinbeiß E 1998 *Phys. Rev. B* **57** 14518
- [9] Renner Ch, Revaz B, Genoud J-K, Kadowaki K, Fischer Ø 1998 *Phys. Rev. Lett.* **80** 149
- [10] Suzuki M, Watanabe T, Matsuda A 1999 *Phys. Rev. Lett.* **82** 5361
- [11] Suzuki M and Watanabe T 2000 *Phys. Rev. Lett.* **85** 4787
- [12] Krasnov V M 2002 *Phys. Rev. B* **65**, 140504
- [13] Latyshev Y I, Yamashita T, Bulaevskii L N, Graf M J, Balatsky A V and Maley M P 1999 *Phys. Rev. Lett.* **82** 5345
- [14] Krasnov V M, Yurgens A, Winkler D, Delsing P and Claeson T 2000 *Phys. Rev. Lett.* **84** 5860
- [15] Stajic J, Iyengar A, Levin K, Boyce B R, Lemberger T R 2003 *Phys. Rev. B* **68** 024520
- [16] Giura M, Fastampa R, Sarti S and Silva E 2004 *Phys. Rev. B* **70** 214530
- [17] Giura M, Fastampa R, Sarti S, Pompeo N and Silva E 2006 submitted to *Physica C* as Proceedings of M2S (Dresden, Germany, July 9th-14th, 2006)

- [18] Poole C P, Farach H A, Creswick R J, 1995 *Superconductivity*, Academic Press, USA, Table A3
- [19] Ma S M 1985 *Statistical Mechanics*, World Scientific.
- [20] Abramowitz M and Stegun I A, eds., 1970 *Handbook of mathematical functions*, 9th printing, Dover publications, INC., New York
- [21] Gradshteyn I S and Ryzhik I M, 1994 *Table of Integrals, Series and Products* (Jeffrey A, editor), Fifth Edition, Academic Press
- [22] Tallon J L, Williams G V M 1999 *Phys. Rev. Lett.* **82** 3725
- [23] Renner Ch, Revaz B, Genoud J-K, Kadowaki K, Fischer Ø 1999 *Phys. Rev. Lett.* **82** 3726
- [24] Krasnov V M, Kovalev A E, Yurgens A, Winkler D 2001 *Phys. Rev. Lett.* **86** 2657
- [25] Krasnov V M, Sandberg M, Zogaj I 2005 *Phys. Rev. Lett.* **94** 077003